

2009

Modulation analysis of boundary induced motion of optical solitary waves in a nematic liquid crystal

Alessandro Alberucci
University of Rome

Gaetano Assanto
University of Rome

Daniel Buccoliero
Australian National University

Anton Desyatnikov
Australian National University

Timothy R. Marchant
University of Wollongong, tim@uow.edu.au

See next page for additional authors

Follow this and additional works at: <https://ro.uow.edu.au/infopapers>



Part of the [Physical Sciences and Mathematics Commons](#)

Recommended Citation

Alberucci, Alessandro; Assanto, Gaetano; Buccoliero, Daniel; Desyatnikov, Anton; Marchant, Timothy R.; and Smyth, Noel: Modulation analysis of boundary induced motion of optical solitary waves in a nematic liquid crystal 2009.
<https://ro.uow.edu.au/infopapers/3306>

Modulation analysis of boundary induced motion of optical solitary waves in a nematic liquid crystal

Disciplines

Physical Sciences and Mathematics

Publication Details

Alberucci, A., Assanto, G., Buccoliero, D., Desyatnikov, A. S., Marchant, T. R. & Smyth, N. F. (2009). Modulation analysis of boundary induced motion of optical solitary waves in a nematic liquid crystal. *Physical Review A (Atomic, Molecular and Optical Physics)*, 79 (043816), 043816-1-043816-8.

Authors

Alessandro Alberucci, Gaetano Assanto, Daniel Buccoliero, Anton Desyatnikov, Timothy R. Marchant, and Noel Smyth

Modulation Analysis of Boundary-Induced Motion of Optical Solitary Waves in a Nematic Liquid Crystal

Alessandro Alberucci,¹ Gaetano Assanto,¹ Daniel Buccoliero,² Anton S. Desyatnikov,² Timothy R. Marchant,³ and Noel F. Smyth⁴

¹*NooEL – Nonlinear Optics and OptoElectronics Lab, Department of Electronic Engineering, CNISM–University of Rome “Roma Tre”, Via della Vasca Navale 84, 00146 Rome, Italy*

²*Nonlinear Physics Center, Research School of Physics and Engineering, The Australian National University, Canberra ACT 0200, Australia*

³*School of Mathematics and Applied Statistics, University of Wollongong, Wollongong, NSW 2522, Australia*

⁴*School of Mathematics and Maxwell Institute for Mathematical Sciences, University of Edinburgh, Edinburgh, Scotland EH9 3JZ, U.K.*

We consider the motion of a solitary wave, a nematicon, in a finite cell filled with a nematic liquid crystal. A modulation theory is developed to describe the boundary induced bouncing of a nematicon in a one dimensional cell and it is found to give predictions in very good agreement with numerical solutions. The boundary induced motion is then considered numerically for a two dimensional cell and a simple extension of the modulation theory from one to two space dimensions is then made, with good agreement being found with numerical solutions for the nematicon trajectory. The role of nematicon shape and relative position to the boundaries in its evolution is discussed.

PACS numbers: 42.65.Tg, 42.70.Df

I. INTRODUCTION

Spatial solitons are ubiquitous as they are found and studied in fluids, plasmas, Bose-Einstein condensates, electronics and optics [1–7]. In optics, in particular, they have received much attention due to the versatile nature of self-induced waveguides, a concept amenable to applications in applied nonlinear optics and communications, for which all-optical switching and routing could play an important role in future generations of signal processors [6–9]. In this scenario, nematicons — i.e. spatial optical solitons in nematic liquid crystals [10, 11] — have stirred attention as a convenient playground for a number of fundamental and applied properties of optical solitons, including the role of nonlocality, not only as a stabilizing mechanism which prevents catastrophic collapse in two transverse dimensions, but also as a long-range link between two or more nematicons, nematicons and extra beams, and nematicons and perturbations, including the boundaries of a cell [12–15]. This latter aspect, i.e. the effect of a nonlocal boundary potential on the propagation of spatial solitons, has been recently addressed with specific reference to thermo-optical and reorientational solitons in glass and in liquid crystals, respectively [16–20]. In this paper we undertake the ambitious task of providing a theoretical background to describe the boundary-nematicon interaction, analysing the boundary induced motion of these self-localized beams by means of modulation theory, modelling the problem in one transverse dimension, but extending some of the results to the full two-dimensional scenario.

II. GOVERNING EQUATIONS

We consider a coherent, polarised light beam inputted into a planar liquid crystal cell, with the z coordinate along the cell and the (x, y) coordinates orthogonal to this direction. Let us take the light to be linearly polarised as an extraordinary wave in the x direction. In one of the experimental scenarios, the optic axis (or molecular *director*) of the nematic liquid crystal (nlc) is prepared parallel to z and a static electric field is applied in the x direction to orient it at an angle $\hat{\theta}$ to the z direction in the absence of light. In this case the extraordinary polarization of the input results in a perturbation of the director angle from the pre-tilt θ due to the light beam launched along z . In non-dimensional form the equations governing the propagation of light through such a liquid crystal cell are then

$$\begin{aligned} i \frac{\partial E}{\partial z} + \frac{1}{2} \nabla^2 E + E \sin 2\theta &= 0, \\ \nu \nabla^2 \theta - q \sin 2\theta &= -2|E|^2 \cos 2\theta, \end{aligned} \quad (1)$$

where the Laplacian ∇^2 is in the (x, y) plane [13, 21]. The variable E is the complex-valued, slowly varying envelope of the optical electric field. The nonlocality ν measures the strength of the response of the nematic in space, with a highly nonlocal response corresponding to ν large. It should be noted that the electric field E in equation (1) has had a phase factor taken out, this factor accounting for the birefringent walk-off due to the Poynting vector of the extraordinary-wave beam deviating from its wavevector [22]. In the nonlocal, ν large limit, it can be seen from the director equation in (1) that θ , the optically induced deviation of the director angle from $\hat{\theta}$, is small. The parameter q is related to the energy (squared amplitude) of the static electric field which pre-tilts the

nematic dielectric [13].

Another experimental scenario, the one which is subject of this work, consists of a cell for which no static pre-tilt field is applied, preparing (“rubbing”) the boundaries of the cell so that the director makes an angle $\hat{\theta}$ with respect to the z direction in the plane yz [23–25]. Therefore, at equilibrium in the absence of the optical field, the director is at an angle $\hat{\theta}$ throughout the cell. When a light beam is launched with wavevector along z , the optical director is then perturbed by a further angle θ . Hence setting $q = 0$ (no static field) in (1) and also taking $|\theta| \ll 1$, which is valid in the highly nonlocal limit, the nematicon equations (1) become

$$i\frac{\partial E}{\partial z} + \frac{1}{2}\nabla^2 E + 2E\theta = 0, \quad \nu\nabla^2\theta = -2|E|^2. \quad (2)$$

The boundary condition for the nematic director at the cell walls is $\theta = 0$.

III. ONE SPACE DIMENSION

Due to the mismatch between the geometries of the rectangular cell and the usual circular Gaussian light beam, it is extremely difficult to perform any analytical analysis for nematicons propagating in two space dimensions. To obtain insight into nematicon evolution in a finite cell without the presence of a static pre-tilting field, let us consider nematicon evolution in one space dimension, so that the optical field evolution is in the plane yz . An added complication with studying nematicons is that there is no known exact analytical solitary wave (nematicon) solution of the nematicon equations. Due to this, it has been found that a powerful approximate technique for studying this problem is that based on trial functions in variational formulations of the governing equations [26–29], this being an extension of modulation theory [30]. This technique is adapted and used in the present work.

The nematic equations (2) have the Lagrangian

$$L = i(E^*E_z - EE_z^*) - |\nabla E|^2 + 4\theta|E|^2 - \nu|\nabla\theta|^2. \quad (3)$$

The success of variational techniques depends on the choice of trial functions. The appropriate choice for nematicons, especially in one space dimension, is the hyperbolic secant profile

$$E = a \operatorname{sech} \frac{y - \xi}{w} e^{i\sigma + iV(y - \xi)} + ig e^{i\sigma + iV(y - \xi)}, \quad (4)$$

where the parameters a , w , σ , V , ξ and g are functions of z . a is the amplitude of the beam, w its width and σ the phase. g is the amplitude of the radiation bed [31]. The first term in this trial function represents a varying nematicon-like beam, while the second term represents the diffractive radiation of low wavenumber which accumulates under the evolving nematicon [27, 31]. This

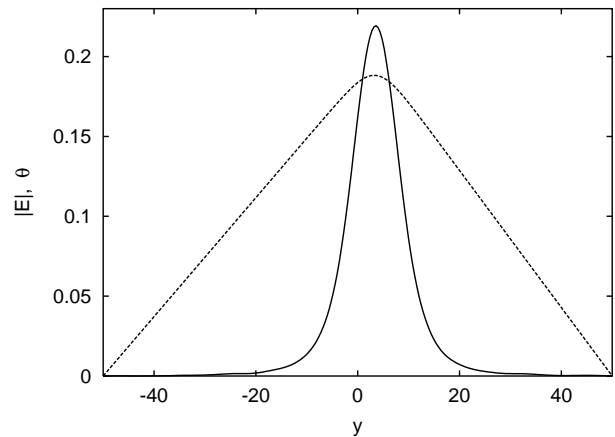


Figure 1: Electric field intensity and director response versus y . Shown are numerical solutions for $|E|$ (solid line) and θ (dashed line) versus y at $z = 2000$. The initial values are $a = 0.2$, $w = 5$, $\xi = 5$ with $\nu = 100$ and $L = 50$.

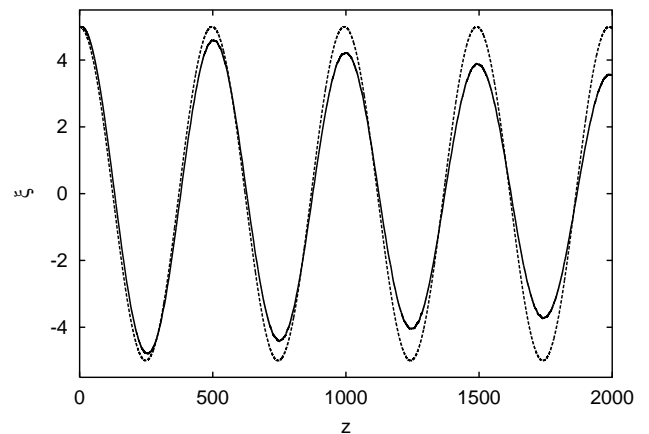


Figure 2: The position of the nematicon peak versus z . Shown are ξ from the numerical solution (solid line) and the modulation solution (dashed line). The initial conditions are $a = 0.2$, $w = 5$, $\xi = 5$ with $\nu = 100$ and $L = 50$.

radiation cannot remain flat, so it is assumed that g is non-zero in the interval $-\ell/2 \leq y \leq \ell/2$ [27, 31].

Substituting the optical field form (4) into the director equation, the second of (2), and using the one space dimensional boundary condition $\theta = 0$ at the cell walls $y = \pm L$ gives the solution

$$\begin{aligned} \nu\theta &= -a^2w^2 \left(1 + \frac{y}{L}\right) \ln s_- - a^2w^2 \left(1 - \frac{y}{L}\right) \ln s_+ \\ &+ 2a^2w^2 \ln \operatorname{sech} \frac{y - \xi}{w}, \end{aligned} \quad (5)$$

$$\text{where } s_+ = \operatorname{sech} \frac{L + \xi}{w}, \quad s_- = \operatorname{sech} \frac{L - \xi}{w},$$

for the director. The peak of the director distribution (5) does not, in general, occur at the location of the electric

field peak $y = \xi$ [14], but at

$$y_m = \xi + w \tanh^{-1} \left(\frac{w}{2L} \ln \frac{s_-}{s_+} \right). \quad (6)$$

Let us set $\alpha_1 = \theta(y_m, z)$ as the amplitude of the director solution (5) at z , which occurs at (6). When the nematic is at the centre of the cell $\xi = 0$, then the director beam has a symmetric form too with $y_m = 0$. In cases when $\xi \neq 0$, however, the peak of the director beam is a little closer to the centre of the cell than the electric field peak, as $|y_m| < |\xi|$.

Applying the modulation method [28, 30, 31], based on the trial function (4) and the director solution (5), then gives the modulation equations governing the evolution of the nematic. These equations and a short discussion of them are given in the Appendix.

IV. RESULTS AND DISCUSSION

A. 1D nematic bouncing in a cell

In this section approximate and numerical solutions of the nematic equations (2) for a (1 + 1) dimensional nematic cell are compared. The (1+1)D numerical solutions were found using the Dufort-Frankel finite difference scheme to solve the electric field equation, the first of (2). For the director equation, the second of (2), Gauss-Seidel iteration was used with successive over relaxation. An advantage of the Dufort-Frankel and Gauss-Seidel schemes is that they are both explicit methods with low storage costs. The step sizes used were $\Delta y = 0.4$ and $\Delta z = 4 \times 10^{-3}$. Note that $\Delta z/\Delta y$ must be small to ensure consistency of the DuFort-Frankel finite difference scheme.

Figure 1 shows the electric field intensity, $|E|$, and the director response, θ , versus y at $z = 2000$. The initial values are $a = 0.2$, $w = 5$, $\xi = 5$ with $\nu = 100$ and $L = 50$. This figure shows that the electric field has the form of a localised beam, while the director response is not localised and has a “near triangular” form, as found by Alberucci and Assanto [18]. The initial location of the beam is not at the centre of the cell, $y = 0$, but is at $y = \xi = 5$. The nematic then oscillates about the centre line of the cell, as found in previous work [14, 19, 20, 22]. At $z = 2000$ the electric field beam is peaked at $y = 3.55$, while the director beam is peaked at $y = 3.24$, a little closer to the centre of the cell than the electric field peak. The electric field amplitude is $a = 0.219$ and the director amplitude is $\alpha_1 = 0.188$. Using the initial values for the parameters and $\xi = 3.55$ in (6) gives $y_m = 3.24$. Hence the analytical expression for the location of the director beam gives an excellent prediction which closely matches the numerically obtained location.

Qualitatively this solution is quite different to the nematic that occurs in the presence of a static pre-tilting electric field applied to overcome the Fréedericksz thresh-

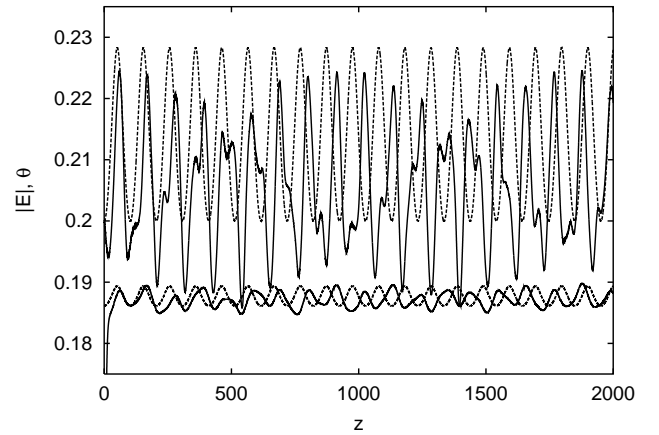


Figure 3: Peak electric field amplitude and director amplitude versus z . Shown are a (upper dashed line) and α (lower dashed line) from the modulation solution and $|E|$ (upper solid line) and θ (lower solid line) from the numerical solution. The initial conditions are $a = 0.2$, $w = 5$, $\xi = 5$ with $\nu = 100$ and $L = 50$.

old [13]. In that case both the electric field and the director response take the form of beams [13], while for the rubbed case the director response is not localised. The reason for these differing behaviours can be deduced from the director equation, the second of (1), applicable when there is a pre-tilting field. We consider the region where the optical electric field is zero ($E = 0$) and assume that θ is small. In this limit the director equation is $\theta_{yy} - (2q/\nu)\theta = 0$, which has the bounded solution

$$\theta = e^{-\sqrt{\frac{2q}{\nu}} y}, \quad (7)$$

for $y > 0$, describing the exponential decay of the director tail in the nonlocal regime for a nematic in the presence of a pre-tilting field. In the rubbed case $q = 0$ the director equation becomes $\theta_{yy} = 0$ far from the optical field, which has a linear solution. The linear regions of the director solution far from the optical field can be clearly seen in Fig. 1.

Figure 2 shows the location of the nematic peak versus z . Shown are ξ from the modulation solution and the corresponding numerical solution. The initial conditions are $a = 0.2$, $w = 5$, $\xi = 5$ with $\nu = 100$ and $L = 50$. The nematic oscillates about the centre line of the cell, this behaviour being previously shown theoretically and numerically for liquid crystals [18, 19, 22] and thermo-optic media [17]. The modulation solution is an undamped periodic solution (nonlinear oscillator) with a wavelength of $z = 497$. Numerically the position oscillates with a wavelength of $z = 500$ and is decaying to $\xi = 0$ on a very long z scale. Assuming exponential decay, the position oscillation would take until $z = 27,000$ to reach 1% of its original value. The comparison between the two solutions is excellent for shorter z values, but for extremely large values of z the modulation solution deviates from the numerical one as diffractive radiation loss has

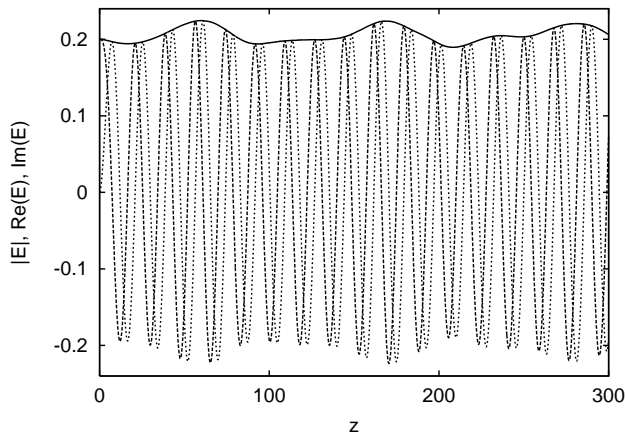


Figure 4: Electric field amplitude versus z . Shown are a (solid line), $\text{Re}(E)$ (large dashes) and $\text{Im}(E)$ (short dashes) from the numerical solution. The initial conditions are $a = 0.2$, $w = 5$, $\xi = 5$ with $\nu = 100$ and $L = 50$.

not been included in the modulation equations. In the present non-dimensional variables typical cell lengths are around 500, so for most realistic experimental scenarios these length scales for decay of the position oscillation are far longer than the length of the liquid crystal cell [10].

Figure 3 shows the peak electric field amplitude and director response amplitude versus z . Shown are a and α_1 from the modulation solution and the corresponding numerical solution. The parameters are $a = 0.2$, $w = 5$, $\xi = 5$ with $\nu = 100$ and $L = 50$. The peak of the numerical electric field oscillates between $a = 0.186$ and 0.224 with a wavelength of $z = 108$. The corresponding director amplitude oscillation is between $\alpha_1 = 0.185$ and 0.189 . The modulation solution predicts a periodic solution with the electric field amplitude oscillating between $a = 0.2$ and $a = 0.228$ with wavelength $z = 103$. The modulation director amplitude oscillates between $\alpha_1 = 0.186$ and 0.189 . These comparisons between the solutions are excellent, except that beating of the numerical electric field amplitude occurs. This is due to a second harmonic component being present in the numerical solution for the nematicon, which is not accounted for in the trial function (4). This second harmonic decays on a very long z scale, much larger than a typical cell length, with the nematicon amplitude oscillation settling down to a harmonic oscillation with a single frequency.

Figure 4 shows the electric field amplitude versus z . Shown are a , $\text{Re}(E)$ and $\text{Im}(E)$ from the numerical solution. This figure shows that the real and imaginary parts of the electric field oscillate between ± 0.2 on a much shorter z -scale than does the electric field amplitude a (for $|E|$), which forms the envelope of the other curves. Numerically, the oscillations in the real and imaginary parts of the electric field have wavelength $z \approx 17$, while the amplitude of $|E|$ oscillates with wavelength $z \approx 109$. The modulation equations give the propagation constant

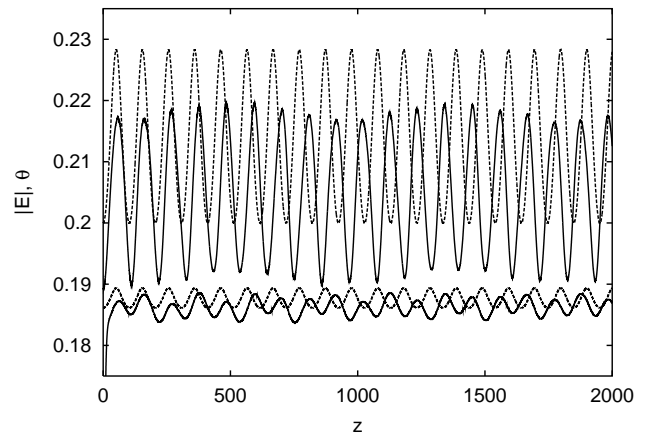


Figure 5: Electric field amplitude and director amplitude versus z . Shown are a (upper dashed line) and α (lower dashed line) from the modulation solution and $|E|$ (upper solid line) and θ (lower solid line) from the numerical solution. The Gaussian initial condition (8) is used with $a_1 = 0.1893$, $\gamma = 0.01274$, $\xi = 5$, $\nu = 100$ and $L = 50$.

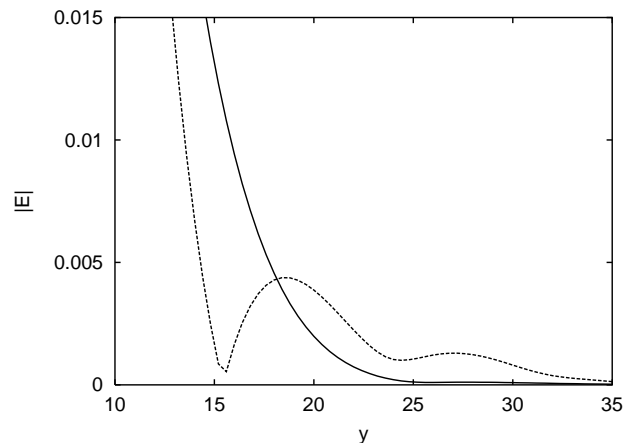


Figure 6: Electric field amplitude $|E|$ versus y . Shown are numerical solutions for the nematicon tail. The Gaussian profile (solid line) is at $z = 435$ and the sech profile (dashed curve) is at $z = 428$. The parameters are $a_1 = 0.1893$, $\gamma = 0.1274$, $a = 0.2$, $w = 5$, $\xi = 0$, $\nu = 100$ and $L = 50$.

σ , which generates the oscillations in the real and imaginary parts of the electric field. Assuming that the beam is near the steady-state ($V = \xi = 0$), then (A14) gives $d\sigma/dz = 0.36$ for this example. This corresponds to a wavelength of 17.5, which is very close to the numerically obtained wavelength.

It can also be seen that the oscillations of the real and imaginary parts of the electric field are not purely harmonic, but undergo beating, which leads to the much smaller amplitude oscillations in the wave envelope $|E|$, which represents the modulus of the electric field. Non-linear effects are generating small contributions from higher harmonics, which lead to the beating of the wave

envelope, as seen in Figs. 3 and 4.

To investigate the beating phenomena further we considered an alternative Gaussian initial condition

$$E = a_1 e^{-\gamma(y-\xi)^2} \quad (8)$$

for the numerical solutions. To obtain a sensible comparison with the modulation solution, which is based on the sech initial condition, the difference between the sech and Gaussian initial profiles was minimised using the method of least squares. For the example illustrated in Figs. 1–4 the parameters $a = 0.2$ and $w = 5$ were used for the sech profile. The method of least squares gives $a_1 = 0.1893$ and $\gamma = 0.01274$ as the parameters of the equivalent Gaussian profile. The Gaussian profile is a little broader at moderate values of y , but decays much faster for large values of y than does the sech profile.

Figure 5 shows the electric field amplitude and director response amplitude versus z . Shown are a and α_1 from the modulation solutions and the corresponding numerical solutions. The initial profile is Gaussian with $a_1 = 0.2$ and $\gamma = 0.01273$. The other parameters are $\xi = 5$, $\nu = 100$ and $L = 50$. The numerical electric field amplitude oscillates between $a = 0.190$ and 0.220 with a wavelength of $z = 110$. The corresponding director amplitude oscillation is between $\alpha_1 = 0.185$ and 0.189 . The modulation solution predicts a periodic solution with the electric field amplitude oscillating between $a = 0.2$ and $a = 0.228$ with wavelength $z = 103$. The director amplitude given by the modulation solution oscillates between $\alpha_1 = 0.186$ and 0.189 . As for the sech profile used for Fig. 3, the comparisons between these solutions are excellent. For the Gaussian profile, however, the beating is much reduced, with the oscillatory pattern of the numerical solution much closer to the constant amplitude oscillations of the modulation solution. The position of the nematicon peak for the Gaussian case is the same, to graphical accuracy, as the position in the sech case illustrated in Fig. 2.

Figure 6 shows the numerical nematicon tail versus y for both the Gaussian (at $z = 435$) and sech (at $z = 428$) profiles. The parameters are $a_1 = 0.1893$, $\gamma = 0.1274$, $a = 0.2$, $w = 5$, $\xi = 0$, $\nu = 100$ and $L = 50$. The z values correspond to minima of the nematicon amplitude, so that the z values differ slightly. Also $\xi = 0$ initially was chosen so that both nematicons are located at the centre of the cell. The figure shows that the sech profile generates much more diffractive radiation, as indicated by the more pronounced oscillations in its tail, while the Gaussian profile shows little shed diffractive radiation. It should be noted, however, that in absolute terms both profiles shed little radiation, in agreement with experiments [25]. The enhanced shedding of diffractive radiation by the sech profile is the reason for the enhanced beating of the amplitude of the sech profile compared with that of the Gaussian profile. This enhanced radiation shedding is associated with a greater evolution of the beam profile as it propagates.

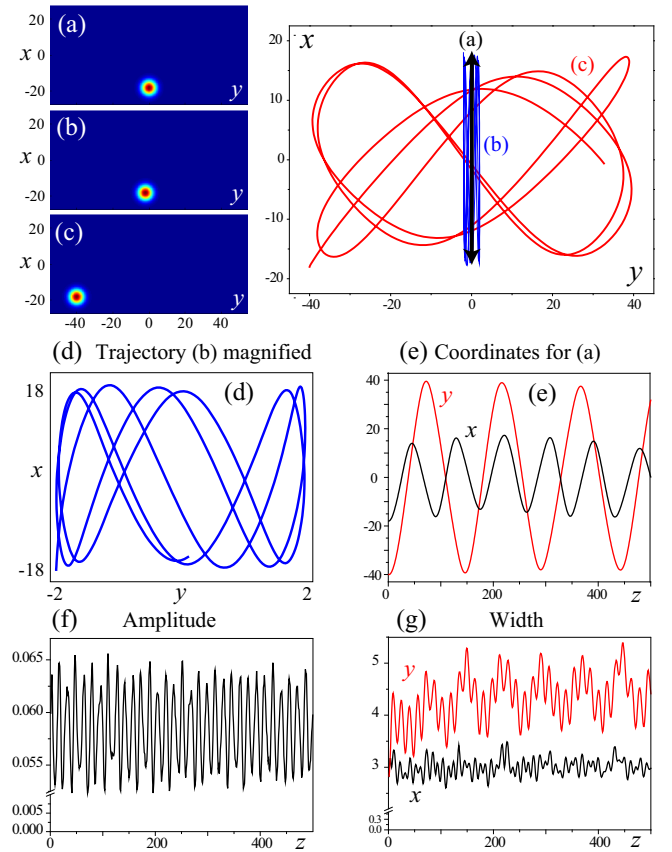


Figure 7: Color online. (a–c) Intensity distributions (left) and nematicon trajectories (right) for three different initial positions of a Gaussian input beam, the colours for intensity are mapped from zero (blue) to maximal value (red). (d) Magnified trajectory (b). (e) Coordinates, (f) amplitude, and (g) widths of the nematicon on the trajectory (c); red lines: y -direction, black lines: x -direction.

B. 2D soliton bouncing in a rectangular cell

Let us now study the propagation of a two dimensional beam in a rectangular cell. To solve the nematicon equations (2) and simulate beam propagation, we employed the split-step fast Fourier transform algorithm, with the director equation, a Poisson equation, being solved at each propagation step. The condition $\theta = 0$ was applied to all four boundaries.

We investigated the trajectories of a nematicon in a rectangular shaped sample with aspect ratio two for three different cases, i.e. we launched the nematicon from three different positions (x_0, y_0) . In all cases we launched the beam adjacent to the elongated boundary, keeping $x_0 = -18$, see Fig. 7(a)–(c), and varied the position in the horizontal direction, with $y_0 = 0, -2$ and -40 . When the beam was placed in the center of the cell with $y_0 = 0$, as shown in Fig. 7(a), the induced refractive index profile was symmetric in the y -direction, see Fig. 8(a), and thus the effective forces from the opposing y boundaries compensated each other. However, due to the induced asym-

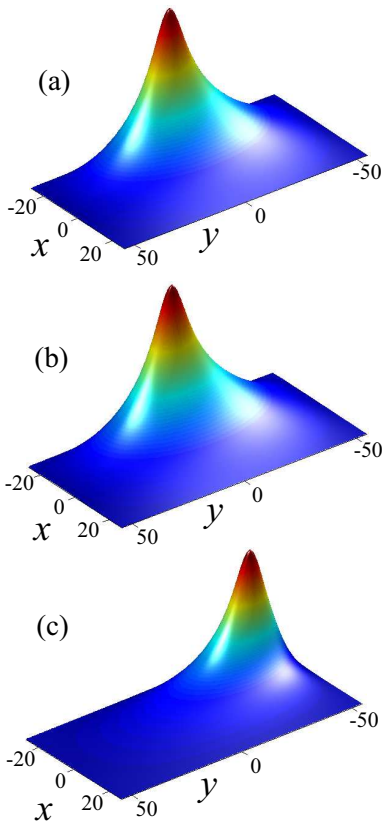


Figure 8: Color online. Refractive index profiles induced by the soliton at various input positions as in Fig. 7.

metry [18, 19] in the gradient of the transverse profile of the director response in the y direction, see Fig. 8(a), the beam is repelled by the boundary and the nematicon moves in the vertical, x direction, periodically bouncing from one side of the sample to the other as it propagates.

This behaviour changes markedly, however, when we launch the input beam shifted slightly off the centre with $y_0 = -2$, see Fig. 7(b). As a consequence of this displacement, the induced potential well, the director profile in Fig. 8(b), is now both horizontally and vertically asymmetric and exerts a net force in both transverse directions. The force exerted by the farther away, vertical boundary is correspondingly smaller and the velocity of the nematicon is therefore much higher in the vertical direction. This, in turn, causes the nematicon to follow a steep trajectory, the blue line in Fig. 7(b) and the inset, which clearly shows that despite being launched very near the center, the nematicon can reach and bounce off the upper, horizontal boundary before the middle of the cell is reached.

Lastly the nematicon was launched near the corner of the sample, see Fig. 7(c). We immediately notice that the repelling effect of the vertical boundary is considerably stronger, which is evident when comparing Figs. 8(b) and (c). In contrast to the previous case, the nematicon actually crosses the center of the cell before the opposite hori-

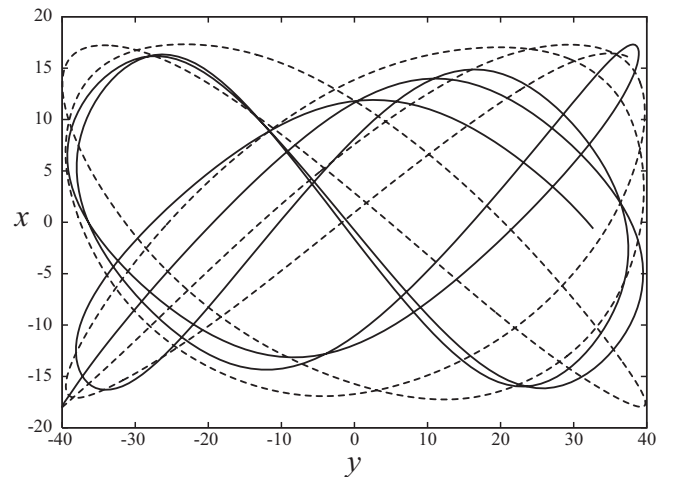


Figure 9: Comparison between trajectories of a nematicon in a two dimensional cell for the initial conditions of Fig. 7(c). Numerical solution: solid line, modulation solution: dashed line.

zontal boundary is reached. The dynamics of the beam in this case is further demonstrated in Figs. 7(e)–(g), where we plot the two spatial positions in the y (red line) and x (black line) directions (e), the beam amplitude (f), and the two full nematicon widths in both directions (y , red, and yx , black) (g). Note that the degree of ellipticity of the beam is comparable with the ratio of the lengths of the cell boundaries.

We note that, for both non-symmetric launch conditions, once the nematicon crosses the middle of the cell it slows down and eventually turns around due to the repelling force of the opposite boundary [18]. This repulsion is a direct consequence of the nonlocal nature of the nematic response, combined with the intricate dependence of the response on the specific properties of the boundaries. In general, boundaries affect not only the position, but also the internal dynamics [20] of more complex soliton of different symmetries [32].

The modulation theory derived in Section 3 and the Appendix was for the case of a one dimensional nematicon. Equivalent modulation equations cannot be derived in $2+1$ dimensions due to the mismatch in symmetry between the rectangular cell and the elliptical beam. However, a simple extension of the one dimensional modulation equations can be made which gives unexpectedly good agreement with numerical solutions and gives insight into the oscillation of the beam in the cell. This simple extension of the one dimensional equations is made by adding a x momentum equation equivalent to the y momentum equation (A4). The resulting trajectory is compared with the numerical one in Fig. 9 for the case shown in Fig. 7(c). In comparing the numerical and theoretical trajectories it should be remembered that the numerical trajectory is for a Gaussian beam and the theoretical one for a sech beam. It can be seen that while there is not detailed agreement, the overall trends and

shapes of the trajectories are consistent. In particular the positions of maximum deviation from the middle of the cell have a good match. The differences in detail between the trajectories are due, in part, to the sech beam having a much slower decay than a Gaussian beam, so that it has a stronger interaction with the boundaries.

CONCLUSIONS

In conclusion, the dynamics of a nematicon influenced by the effective forces resulting from the boundaries of a liquid crystal cell was studied both analytically and numerically. Particular emphasis was placed on this dynamics when the position of the nematicon within the cell was non-symmetric. The physical reason for this boundary effect lies in the interaction of the nematicon tails with the boundaries and the consequent creation of an effective repulsive potential. For a one-dimensional nematicon we developed a modulation theory and verified its predictions by direct numerical simulations. In particular, we discussed the influence of the nematicon profile,

namely the decay rate of its tails, on the motion of a nematicon, as well as on its oscillation dynamics. We extended our investigation to the two-dimensional case with equal boundary conditions on all the rectangular boundaries of the cell, for which the results of numerical simulations were compared with the 2 dimensional generalization of the modulational analysis. We found good qualitative agreement in the description of the 2 dimensional nematicon motion and discussed the reasons for the quantitative discrepancies.

This research was supported by the Engineering and Physical Sciences Research Council (EPSRC) under grant EP/D075947/1 and by the Australian Research Council.

Appendix: Shelf Radius

Applying the modulation method [28, 30, 31], based on the trial function (4) and the director solution (5), gives the modulation equations

$$\frac{d}{dz} [2a^2w + \ell g^2] = 0, \quad (\text{A1})$$

$$\pi \frac{d}{dz} (aw) = \ell g \left(\frac{d\sigma}{dz} - \frac{1}{2}V^2 \right), \quad (\text{A2})$$

$$\begin{aligned} \frac{dg}{dz} &= \frac{2}{3\pi} \frac{a}{w^2} - \frac{2a^3w^3}{\pi\nu L} \left(\ln \frac{s_+}{s_-} \right)^2 - \frac{4a^3w(L-\xi)}{\pi\nu} \left(1 - \frac{1}{2}s_-^2 \right) \\ &\quad - \frac{4a^3w(L+\xi)}{\pi\nu} \left(1 - \frac{1}{2}s_+^2 \right) + \frac{2a^3w^2}{\pi\nu L} \ln \left(\frac{s_+}{s_-} \right) [(L-\xi)t_- - (L+\xi)t_+] \\ &\quad - \frac{4a^3w^2}{\pi\nu} \left[\ln(1-t_-) - \ln s_- + \frac{1}{2}t_- + \ln(1-t_+) - \ln s_+ + \frac{1}{2}t_+ \right], \end{aligned} \quad (\text{A3})$$

$$\frac{d}{dz} [(2a^2w + \ell g^2)V] = \frac{2a^4w^3}{\nu L} \ln \left(\frac{s_+}{s_-} \right) [t_- + t_+] + \frac{2a^4w^2}{\nu} [s_-^2 - s_+^2], \quad (\text{A4})$$

$$\frac{d\xi}{dz} = V, \quad (\text{A5})$$

$$\begin{aligned} \frac{dH}{dz} &= \frac{d}{dz} \left\{ \frac{2}{3} \frac{a^2}{w} + \frac{8a^4w^2L}{\nu} + \frac{2a^4w^4}{\nu L} \left(\ln \frac{s_+}{s_-} \right)^2 + (2a^2w + \ell g^2)V^2 \right. \\ &\quad \left. - \frac{8a^4w^3}{\nu} \left[\ln s_- - \ln(1-t_-) - \frac{1}{2}t_- - \ln(1-t_+) + \ln s_+ - \frac{1}{2}t_+ \right] \right\} = 0, \end{aligned} \quad (\text{A6})$$

$$\begin{aligned} \frac{d\sigma}{dz} - \frac{1}{2}V^2 &= -\frac{1}{2w^2} - \frac{4a^2wL}{\nu} - \frac{a^2w^2}{\nu L} \ln \left(\frac{s_+}{s_-} \right) [(L-\xi)t_- - (L+\xi)t_+] \\ &\quad + \frac{2a^2w^2}{\nu} \left[-\ln(1-t_-) + \ln s_- - \frac{1}{2}t_- - \ln(1-t_+) + \ln s_+ - \frac{1}{2}t_+ \right] \\ &\quad + \frac{2a^2w(L-\xi)}{\nu} \left(1 - \frac{1}{2}s_-^2 \right) + \frac{2a^2w(L+\xi)}{\nu} \left(1 - \frac{1}{2}s_+^2 \right), \quad \text{where} \end{aligned} \quad (\text{A7})$$

$$s_+ = \operatorname{sech} \frac{L+\xi}{w}, \quad s_- = \operatorname{sech} \frac{L-\xi}{w}, \quad t_+ = \tanh \frac{L+\xi}{w}, \quad t_- = \tanh \frac{L-\xi}{w}.$$

These modulation equations do not include loss to diffractive radiation [28, 31] as it has been observed experimentally [25] and from theoretical solutions [29] that on the length scales of a typical cell this loss is very small and can be ignored. This point is taken up further in the Results and Discussions section. The modulation equation (A1) is the equation for conservation of mass, (A4) is the momentum equation and (A6) is the equation for conservation of energy in the sense of invariances of the Lagrangian for the nematicon equations.

The modulation equations (A1)–(A7) have a fixed point for a steady nematicon. Denoting fixed point values with a $\hat{\cdot}$ superscript, $\hat{\xi} = 0$, $\hat{V} = 0$ and $\hat{g} = 0$. The modulation equation (A3) gives the steady amplitude as

$$\frac{\nu}{6\hat{w}^4\hat{a}^2} = 2 \ln(1 - \tanh \tilde{L}) - 2 \ln \operatorname{sech} \tilde{L} + \tanh \tilde{L} + 2\tilde{L} \tanh^2 \tilde{L} + \tilde{L} \operatorname{sech}^2 \tilde{L}, \quad (\text{A8})$$

here $\tilde{L} = L/\hat{w}$. It should be noted that when the nematicon is far from the cell walls $L \gg \hat{w}$, and it can be easily found that in this limit the fixed point relation has a physical solution. Using this relation between \hat{a} and \hat{w} , the fixed point is determined from the boundary condition at $z = 0$ on using the conserved energy (A6).

The final parameter to determine is the shelf length ℓ . The usual method of determining this parameter is to linearise the modulation equations about their fixed point, which results in a simple harmonic oscillator equation [28, 31]. The frequency of this oscillator is then matched to the solitary wave frequency, determining ℓ [28, 31]. However this method was found not to work for the present modulation equations. This is because in the previous cases the perturbation in the nematic formed a beam, which is not the case here, as can be seen from Fig. 1. The shelf length ℓ was then found from numerical solutions by matching the oscillation frequency of

the solution of the modulation equations (A1)–(A7) to the numerical oscillation frequency for a particular initial condition, giving $\ell = 0.5\hat{w}$. This value was found to be robust for other initial conditions.

If the nematicon is far from the cell walls, $L \gg w$. In this limit the modulation equations (A1)–(A7) simplify greatly to become

$$\frac{d}{dz} [2a^2w + \ell g^2] = 0, \quad (\text{A9})$$

$$\frac{d}{dz}(aw) = \frac{\ell g}{\pi} \left(\frac{d\sigma}{dz} - \frac{1}{2}V^2 \right), \quad (\text{A10})$$

$$\frac{dg}{dz} = \frac{2}{3\pi} \frac{a}{w^2} - \frac{4a^3w^2}{\pi\nu} - \frac{6a^3w\xi^2}{\pi\nu L}, \quad (\text{A11})$$

$$\frac{d}{dz} [(2a^2w + \ell g^2)V] = -\frac{8a^4w^2\xi}{\nu L}, \quad (\text{A12})$$

$$\frac{d\xi}{dz} = V, \quad (\text{A13})$$

$$\frac{d\sigma}{dz} - \frac{V^2}{2} = -\frac{1}{2w^2} - \frac{2a^2w^2}{\nu} \left[1 - \frac{2L}{w} + \frac{8\xi^2}{L} \right], \quad (\text{A14})$$

$$0 = \frac{dH}{dz} = \frac{d}{dz} \left[\frac{2a^2}{3w} + \frac{8a^4w^3}{\nu} - \frac{8a^4w^2L}{\nu} + \frac{8a^4w^2\xi^2}{\nu L} + (2a^2w + \ell g^2)V^2 \right]. \quad (\text{A15})$$

to exponentially small terms. In this limit the fixed point can also be easily found to be

$$\hat{w}^6 = \frac{2\nu L}{9|H|}, \quad \text{with} \quad \hat{a}^2 = \frac{\nu}{6\hat{w}^4}. \quad (\text{A16})$$

-
- [1] R. K. Dodd, J. C. Eilbeck, J. D. Gibbon, and H. C. Morris, *Solitons and Nonlinear Wave Equations*, Academic Press, New York (1982).
- [2] P. G. Drazin and R. S. Johnson, *Solitons: an Introduction*, Cambridge University Press, New York (1989).
- [3] L. Lamb and J. Prost, *Solitons in Liquid Crystals*, Springer, New York (1991).
- [4] M. J. Ablowitz and P. A. Clarkson, *Solitons, Nonlinear Evolution Equations, and Inverse Scattering*, Cambridge University Press, New York (1991).
- [5] A. C. Newell, *Solitons in Mathematics and Physics*, Soc. Ind. Mathem., New York (1991).
- [6] F. K. Abdullaev, S. Darmanyan, and P. Khabibulaev, *Optical Solitons*, Springer, Berlin (1993).
- [7] Yu. S. Kivshar and G. P. Agrawal, *Optical Solitons: From Fibers to Photonic Crystals* Academic Press, San Diego (2003).
- [8] A. W. Snyder and D. J. Mitchell, “Accessible Solitons,” *Science* **276**, 1538–1543 (1997).
- [9] G. I. Stegeman, D. N. Christodoulides, and M. Segev, “Optical Spatial Solitons: a historical perspective,” *IEEE J. Sel. Top. Quantum Electron.* **6**, 1419–1425 (2000).
- [10] M. Peccianti, G. Assanto, A. De Luca, C. Umeton, and I. C. Khoo, “Electrically Assisted Self-Confinement and Waveguiding in planar Nematic Liquid Crystal cells,” *Appl. Phys. Lett.* **77**, 7–9 (2000).
- [11] G. Assanto, M. Peccianti, and C. Conti, “Nematicons: optical spatial solitons in nematic liquid crystals,” *Opt. Photon. News* **14**, 44–48 (2003).
- [12] M. Peccianti, K. A. Brzdukiewicz, and G. Assanto, “Non-local spatial soliton interactions in bulk nematic liquid crystals,” *Opt. Lett.* **27**, 1460–1462 (2002).
- [13] C. Conti, M. Peccianti and G. Assanto, “Route to nonlocality and observation of accessible solitons,” *Phys. Rev. Lett.* **91**, 073901 (2003).
- [14] C. Conti, M. Peccianti and G. Assanto, “Observation of optical spatial solitons in a highly nonlocal medium,” *Phys. Rev. Lett.* **92**, 113902 (2004).
- [15] C. Conti, M. Peccianti, and G. Assanto, “Complex dy-

- namics and configurational entropy of spatial optical solitons in nonlocal media,” *Opt. Lett.* **31**, 2030–2032 (2006).
- [16] C. Rotschild, O. Cohen, O. Manela, M. Segev and T. Carmon, “Solitons in Nonlinear Media with an Infinite Range of Nonlocality: First Observation of Coherent Elliptic Solitons and of Vortex-Ring Solitons,” *Phys. Rev. Lett.* **95**, 213904 (2005).
- [17] B. Alfassi, C. Rotschild, O. Manela, M. Segev and D. N. Christodoulides, “Boundary force effects exerted on solitons in highly nonlocal nonlinear media,” *Opt. Lett.* **32**, 154–156 (2007).
- [18] A. Alberucci and G. Assanto, “Propagation of optical spatial solitons in finite-size media: interplay between nonlocality and boundary conditions,” *J. Opt. Soc. Amer. B* **24**, 2314–2320 (2007).
- [19] A. Alberucci, M. Peccianti and G. Assanto, “Nonlinear bouncing of nonlocal spatial solitons at the boundaries,” *Opt. Lett.* **32**, 2795–2797 (2007).
- [20] D. Buccoliero, A. S. Desyatnikov, W. Krolikowski, and Yu. S. Kivshar, “Boundary effects on the dynamics of higher-order optical spatial solitons in nonlocal thermal media,” *J. Opt. A*, in press (2009).
- [21] I. C. Khoo, *Liquid Crystals: Physical Properties and Nonlinear Optical Phenomena*, Wiley, New York (1995).
- [22] M. Peccianti, A. Fratolocci and G. Assanto, “Transverse dynamics of nematicons,” *Opt. Expr.* **12**, 6524–6529 (2004).
- [23] M. Peccianti, C. Conti, G. Assanto, A. De Luca, and C. Umeton, “Routing of Highly Anisotropic Spatial Solitons and Modulational Instability in liquid crystals,” *Nature* **432**, 733–737 (2003).
- [24] A. Alberucci, M. Peccianti, G. Assanto, G. Coschignano, A. De Luca, and C. Umeton, “Self-healing generation of spatial solitons in liquid crystals,” *Opt. Lett.* **30**, 1381–1383 (2005).
- [25] A. Fratolocci, A. Piccardi, M. Peccianti and G. Assanto, “Nonlinear management of the angular momentum of soliton clusters: theory and experiments,” *Phys. Rev. A* **75**, 063835 (2007).
- [26] C. García-Reimbert, A. A. Minzoni and N. F. Smyth, “Spatial soliton evolution in nematic liquid crystals in the nonlinear local regime,” *J. Opt. Soc. Amer. B* **23**, 294–301 (2006).
- [27] C. García-Reimbert, A. A. Minzoni, N. F. Smyth and A. L. Worthy, “Large-amplitude nematicon propagation in a liquid crystal with local response,” *J. Opt. Soc. Amer. B* **23**, 2551–2558 (2006).
- [28] A. A. Minzoni, N. F. Smyth and A. L. Worthy, “Modulation solutions for nematicon propagation in non-local liquid crystals,” *J. Opt. Soc. Amer. B* **24**, 1549–1556 (2007).
- [29] G. Assanto, N. F. Smyth and A. L. Worthy, “Two colour, nonlocal vector solitary waves with angular momentum in nematic liquid crystals,” *Phys. Rev. A* **78**, 013832 (2008).
- [30] G. B. Whitham, *Linear and Nonlinear Waves*, John Wiley and Sons, New York (1974).
- [31] W. L. Kath and N. F. Smyth, “Soliton evolution and radiation loss for the nonlinear Schrödinger equation,” *Phys. Rev. E* **51**, 1484–1492 (1995).
- [32] D. Buccoliero, A. S. Desyatnikov, W. Krolikowski, and Yu. S. Kivshar, “Laguerre and Hermite soliton clusters in nonlocal nonlinear media,” *Phys. Rev. Lett.* **98**, 053901 (2007).